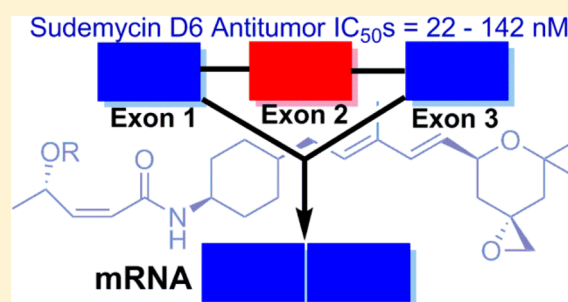


## Optimization of Antitumor Modulators of Pre-mRNA Splicing

Chandraiah Lagisetty,<sup>†,§</sup> Gustavo Palacios,<sup>†,§</sup> Tinopiwa Goronga,<sup>†</sup> Burgess Freeman,<sup>‡</sup> William Caufield,<sup>‡</sup> and Thomas R. Webb<sup>\*,†,||</sup><sup>†</sup>Department of Chemical Biology and Therapeutics, <sup>‡</sup>Preclinical PK Shared Resource, St. Jude Children's Research Hospital, 262 Danny Thomas Place, Memphis, Tennessee 38105-2794, United States

## Supporting Information

**ABSTRACT:** The spliceosome regulates pre-mRNA splicing, which is a critical process in normal mammalian cells. Recently, recurrent mutations in numerous spliceosomal proteins have been associated with a number of cancers. Previously, natural product antitumor agents have been shown to interact with one of the proteins that is subject to recurrent mutations (SF3B1). We report the optimization of a class of tumor-selective spliceosome modulators that demonstrate significant *in vivo* antitumor activity. This optimization culminated in the discovery of sudemycin D6, which shows potent cytotoxic activity in the melanoma line SK-MEL-2 ( $IC_{50}$  = 39 nM) and other tumor cell lines, including JeKo-1 ( $IC_{50}$  = 22 nM), HeLa ( $IC_{50}$  = 50 nM), and SK-N-AS ( $IC_{50}$  = 81 nM). We also report improved processes for the synthesis of these compounds. Our work supports the idea that sudemycin D6 is worthy of further investigation as a novel preclinical anticancer agent with application in the treatment of numerous human cancers.



Our work supports the idea that sudemycin D6 is worthy of further investigation as a novel preclinical anticancer agent with application in the treatment of numerous human cancers.

## INTRODUCTION

In most eukaryotic cells, the splicing of pre-mRNA is a critical process that is catalyzed and regulated by the spliceosome machinery.<sup>1</sup> The spliceosome is a complex of many proteins and RNA that includes five small-nuclear ribonucleoproteins (snRNPs) (U1, U2, U4/U6, and U5) and more than 150 other associated proteins.<sup>2,3</sup> The spliceosome catalyzes removal of noncoded introns from pre-mRNA, joins coded exons together to generate mature RNA, and also controls the process of alternative splicing, which is an important mechanism for regulating cellular function.<sup>4</sup> Two bacterial natural products, FR901464 (FR)<sup>5-7</sup> and pladienolide (PD)<sup>8,9</sup> (Figure 1), have been reported to target the SF3B subunit of the spliceosome.<sup>10,11</sup> Subsequent to those initial discoveries, the list of bacterial natural products targeting the SF3B subunit has grown (Figure 1) to include other bacterial natural products including herboxidiene (GEX1A)<sup>12</sup> (isolated from *Streptomyces* sp. A7847) and the thailanstatins (isolated from *Burkholderia thailandensis*).<sup>13</sup> A similar interaction with the SF3B subunit is also likely for the macrolide natural product FD-895 given its potent biological activity and its high structural and pharmacophore similarity to PD.<sup>14,15</sup> These bacterial fermentation products show cytotoxic  $IC_{50}$ 's in the low nanomolar range in several tumor cell lines and have been reported to have a similar distinctive effect on the cell cycle in mammalian cell lines, including cell cycle arrest in the G1 and G2/M phases.<sup>5,16</sup> Several of these natural products have also been reported to show potent antitumor activity *in vitro* and *in vivo*.<sup>17</sup> Work in this area led to the development of the semisynthetic PD analogue E7107 (Figure 1) for clinical studies.<sup>11</sup>

There is increasing evidence that aberrant splicing of pre-mRNA is a driver of tumorigenesis<sup>4</sup> and that modulation of this process may be a valid target for cancer therapy.<sup>17-20</sup> Subsequent to the characterization of FR and PD as spliceosome modulators, recurrent mutations in SF3B1 were independently identified in myelodysplastic syndromes (MDS),<sup>21</sup> chronic lymphocytic leukemia (CLL),<sup>22</sup> acute myeloid leukemia (AML),<sup>23</sup> and uveal melanoma.<sup>24</sup> The selective sensitivity of tumors to agents such as PD and meayamycin has been the topic of significant research efforts and has very recently been linked to overexpression of MYC<sup>25</sup> or the perturbation of the pre-mRNA splicing of Mcl-1,<sup>26</sup> respectively. Thus, the collective progress in natural-product screening, target identification, and high-throughput transcriptome sequencing has led to a remarkable convergence of independent research areas, which have simultaneously identified new oncology drug targets and new small-molecule therapeutic agents.<sup>17,20</sup>

Numerous total synthetic approaches to FR have been reported, which is one of these active natural products. Most of these syntheses directly target the highly intricate natural product itself or corresponding synthetically complex analogues.<sup>28-32</sup> In spite of much progress, it remains challenging to synthetically access large quantities of the natural-product spliceosome modulators or their close analogues because of the structural complexity and the presence of eight or more stereocenters.<sup>17</sup> As part of our effort to develop a class of druglike and elegant natural-product analogues, we previously

Received: September 6, 2013

Published: December 11, 2013

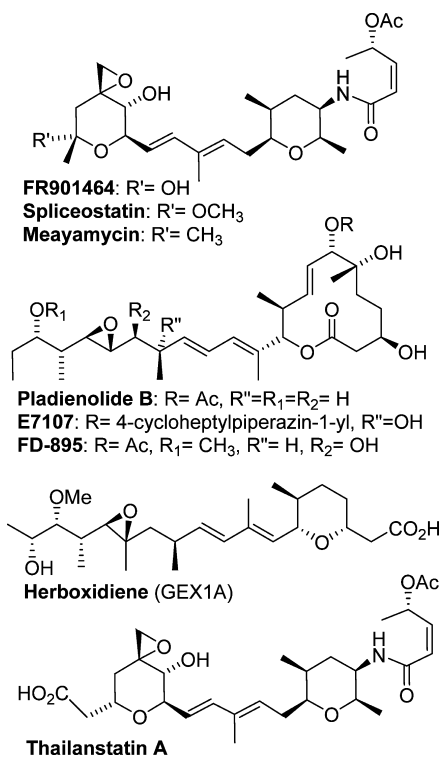


**Figure 1.** Natural product spliceosome modulators (FR901464,<sup>10</sup> pladienolides,<sup>11</sup> herboxidiene,<sup>12</sup> thailanstatins,<sup>13</sup> and FD-895)<sup>15</sup> along with semisynthetic analogues (E7107<sup>11</sup> and spliceostatin<sup>10</sup>) and a structurally similar totally synthetic analogue class (meayamycins).<sup>27</sup>

reported the design and synthesis of FR analogues (the sudemycins)<sup>33–35</sup> and pladienolide analogues,<sup>36</sup> which are active simplified compounds that effectively modulate alternate splicing.<sup>35</sup> Most of our related lead-optimization work has focused on the sudemycins, which are chemically stable synthetic molecules that were designed on the basis of the known FR structure–activity relationships (SAR) and the application of a hypothetical consensus pharmacophore model that is derived from molecular overlays of FR and PD.<sup>33–35</sup>

Although the application of small-molecule splicing modulators may have broad anticancer potential, we chose to focus significant attention on melanoma for the purposes of the present study because melanoma is one of several cancers that

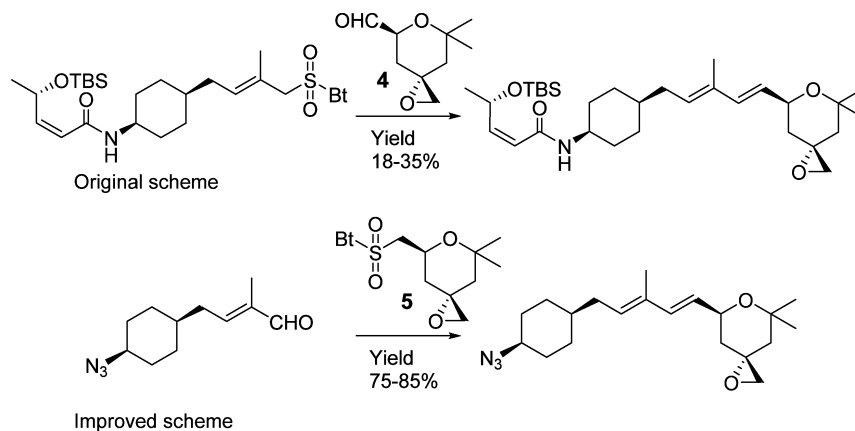
continue to be a major therapeutic challenge in the field of pediatric and adult cancer chemotherapy.<sup>37</sup> We have previously reported the initial SAR with the early generations of these compounds in addition to the initial results of the *in vitro* evaluation of these analogues in a panel of tumor cell lines.<sup>33,34</sup> This work led to the identification of several types of drug-sensitive tumor lines, which included several melanoma lines. Because of this observed drug sensitivity combined with the critical need for new therapeutic agents for melanoma, we have also emphasized *in vivo* experiments with melanoma. As such, melanoma as a model disease serves to exemplify a major potential clinical application for a sudemycin lead candidate. We now report progress in lead-optimization efforts that have led to novel sudemycin analogues possessing *in vivo* activity in a murine melanoma xenograft model. Additionally, we also report the results from *in vitro* dual-agent synergy/antagonism experiments with these newly optimized sudemycin derivatives when combined with a set of approved and investigational antitumor drugs.

In the following, we describe additional SAR results and new compounds that possess important structural modifications required for enhanced *in vivo* antitumor activity. In addition to substantial new data on the biological activity of these compounds, we also report new and substantially improved synthetic processes including the incorporation of a novel sulfone reagent for the key Julia–Kocienski coupling step. The synthetic refinements allow for a much more efficient and scalable process that makes these sudemycin analogues available for clinical development.

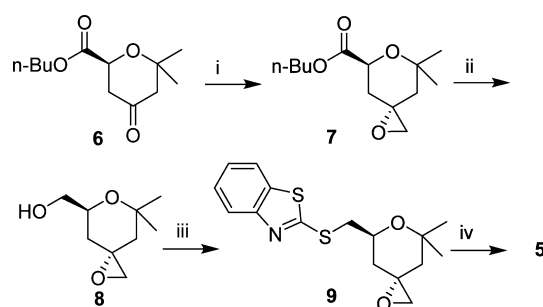
## RESULTS AND DISCUSSION

**Synthesis.** Previously we have reported the practical enantioselective and diastereospecific synthesis of key intermediates for the sudemycin series that includes a key Julia–Kocienski olefination (Scheme 1, top panel).<sup>33,34</sup> Our original synthetic scheme, although quite useful for the synthesis of new analogues, did not represent an efficient process for large amounts of sudemycin analogues for *in vivo* studies. We now report a much improved procedure (Scheme 1, bottom panel, and Scheme 2) using an alternate retrosynthetic dissection,<sup>38</sup> which makes use of the novel and highly crystalline sulfone **5**. As can be seen in Scheme 1, this process gives a much higher overall yield of the key coupling product. As can also be seen in

**Scheme 1.** Comparison of the Original Synthetic Approach to the Sudemycins to the Improved Route<sup>a</sup>



<sup>a</sup>Bt = 2-benzo[*d*]thiazole.

Scheme 2. Optimized Synthetic Approach to Key Intermediate 5<sup>a</sup>

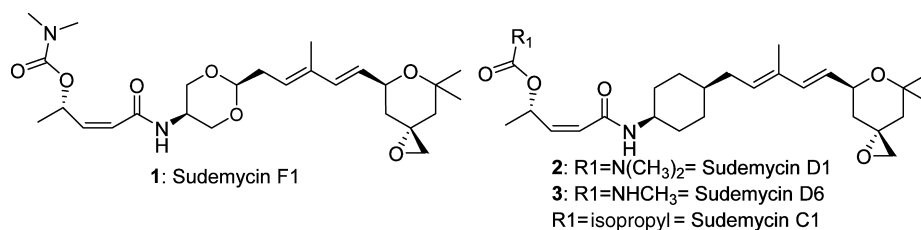
<sup>a</sup>(i) KO<sup>t</sup>Bu, Me<sub>3</sub>SOI, DMSO; (ii) polymethylhydrosiloxane, Ti(O<sup>i</sup>Pr)<sub>4</sub>; (iii) 2-benzthiazoleSH, Ph<sub>3</sub>P, diisopropyl diazodicarboxylate, THF; (iv) ammonium molybdate, 30% H<sub>2</sub>O<sub>2</sub>.

Scheme 2, Julia–Kocienski reagent 5 can be readily derived from the previously reported spiroepoxy alcohol 8.<sup>33</sup> Additional refinements to the synthesis of 5 include the replacement of hazardous NaH with the much more practical potassium *t*-butoxide for the generation of the sulfur ylide in the diastereospecific epoxidation step (to prepare 7, see the Experimental Section). We were also able to replace the hazardous pyrophoric reagent KH with potassium *t*-butoxide as a refinement in the preparation of the intermediate (*S,Z*)-4-((*tert*-butyldimethylsilyloxy)pent-2-enoic acid used in this scheme (see the Supporting Information).<sup>33</sup> A further enhancement in the synthetic process is the replacement of the diisobutyl aluminum hydride with the safer and more cost-effective polymethylhydrosiloxane (PMHS)/Ti(O<sup>i</sup>Pr)<sub>4</sub> combination<sup>39</sup> for the selective reduction of the ester to alcohol in the presence of a spiroepoxide group (Scheme 2). This new route also replaces the *t*-butoxycarbonyl protecting group with azide protection.<sup>40,41</sup> (All synthetic protocols for these improvements are included in the Experimental Section and Supporting Information.) These refinements allow for the practical synthesis of >10 g amounts of sudemycin derivatives in a standard research laboratory setting and will facilitate the development of synthetic processes suitable for larger scale synthesis that will be required for clinical studies.

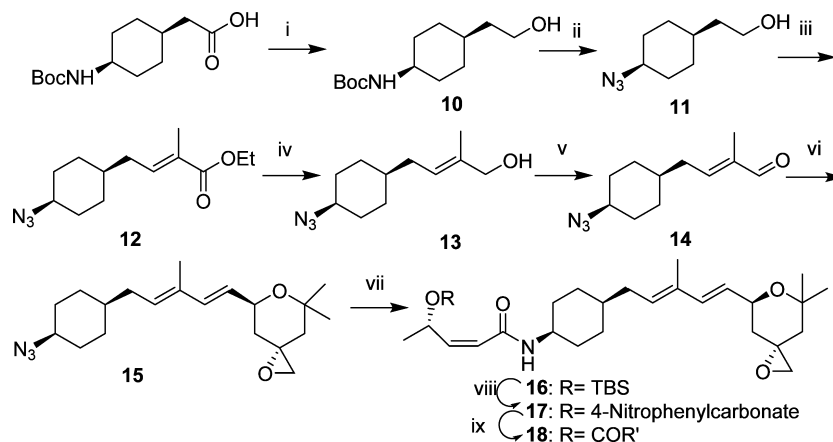
**Structure–Activity Relationships (SAR).** Several factors must be optimized simultaneously to develop a lead compound that displays adequate tumor efficacy in vivo. These factors include (1) potent on-target cell-based activity against the tumor, (2) reasonable metabolic stability (so that the drug will reach the tumor), (3) solubility (so that the drug can be formulated for in vivo delivery), and, importantly, (4) rapid onset of action (so that the drug acts before it is metabolized). The development of a compound that optimizes all of these parameters simultaneously is a significant challenge. In the case

of our spliceosome-modulator lead-optimization work, we identified potency (as measured initially by cytotoxicity and confirmed by potent effects on the modulation of MDM2 splicing), druglike solubility, and rapid onset of cytotoxicity (as measured by drug washout experiments) as the primary initial qualities needed in a candidate drug molecule. Compounds were evaluated by initial screening in a 72 h cytotoxicity against a small panel of tumor cell lines (generally, JeKo1 and PC-3) and were selected for further evaluation on the basis of potency (IC<sub>50</sub> < 250 nM) in one of the cell lines of interest. Finally, the best leads were ranked in order of the most promising solubility and metabolic stability characteristics. We have found the structure–activity of these spliceosome-modulatory compounds to be very sensitive to even small changes in the general scaffolds (derivatives of 1 or 2, shown in Figure 2). Our work<sup>33,34</sup> and previously reported SAR work on analogues that have close structural similarity to FR have shown pronounced limits on the activity tolerance for many structural changes.<sup>27</sup> In these cell-based assays, biological activity can be affected by numerous factors, including transport into the cell and into the nucleus (in order to reach the spliceosome) and cellular metabolic stability in addition to the affinity for the spliceosome. Therefore, many of the modifications that we examined resulted in a significant reduction in cytotoxic activity, presumably by negatively impacting one of these important factors. These analogues were prepared using the previously published chemistry or that shown in Scheme 3.

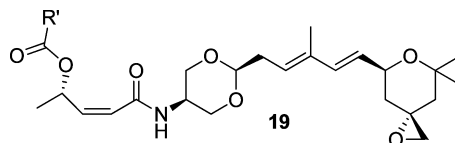
Because FR and our first series of active compounds all contain a metabolically labile ester group, we have previously investigated and reported the activity of the alcohol metabolites of our compounds, which were found to have cytotoxicity IC<sub>50</sub> values of >1 μM against all cell lines examined,<sup>35</sup> consistent with the pharmacophore model that we have previously proposed.<sup>33</sup> Therefore, we have now expanded on our previous reports via the synthesis and evaluation of new ester and optimized carbamate derivatives of the general structure shown in Figure 2 to identify potent compounds with improved solubility and improved metabolic stability.<sup>34</sup> As can be seen by inspection of Table 1, a new ester (19a) and a diverse collection of carbamate derivatives (19b–o) were prepared and screened for cytotoxicity. With regard to the following SAR analysis, our focus was on the identification of potent compounds with IC<sub>50</sub>'s significantly below 1 μM. Because of the inherent error in cytotoxicity measurements, it is possible that some IC<sub>50</sub>'s may actually overlap. However, several general trends can be seen. For example, although some level of substitution was possible, the compounds that contained longer chain groups (or polar solubilizing groups) were less potent than 1. As can be seen by inspection of Table 1 together with our previously published work on carbamate derivatives of 18,<sup>34</sup> there was limited tolerance for the length of the alkyl chains in



**Figure 2.** Structures of the previously reported compounds sudemycin C1<sup>33</sup> and sudemycin F1<sup>35</sup> along with the new preclinical lead compounds sudemycin D1 and D6, which have not previously been disclosed.

Scheme 3. Improved Synthesis of Sudemycin Analogues<sup>a</sup>

<sup>a</sup>(i) Borane/THF, 0 °C to rt; (ii) (1) TFA, (2) K<sub>2</sub>CO<sub>3</sub>, (3) imidazolesulfonyl azide, K<sub>2</sub>CO<sub>3</sub>; (iii) (1) Swern oxidation, (2) ethyl 2-(triphenylphosphoranylidene)propanoate; (iv) DIBAL-H, CH<sub>2</sub>Cl<sub>2</sub>, -78 °C; (v) pyridine, Dess–Martin periodinane; (vi) 5/NaHMDS, THF, -78 °C; (vii) (1) Ph<sub>3</sub>P, H<sub>2</sub>O, 55 °C, (2) 2.DIPEA, HBTU, (*S,Z*)-4-((TBS)oxy)pent-2-enoic acid; (viii) for carbamates (1) TBAF/THF, (2) 4-nitrophenylchloroformate/THF; (ix) R<sub>1</sub>R<sub>2</sub>NH/THF or R''COCl/pyr for esters.

Table 1. SAR of the New Ester and Carbamate Derivatives Prepared Using Previously Reported Procedures<sup>a</sup>

R'	ID	JeKo1	PC3	R'	ID	JeKo1	PC3
-C(CH <sub>3</sub> ) <sub>3</sub>	19a	0.34	1.2	<i>N</i> -methyl- <i>N</i> - <i>t</i> -butylamine	19i	0.78	2.7
<i>n</i> -butylamine	19b	>1	>10	morpholine	19j	1.32	7.8
diethylamine	19c	>1	>10	piperidine	19k	1.47	7.2
<i>t</i> -butylamine	19d	>1	7.3	pyrrolidine	19l	0.97	4.6
<i>N</i> -methyl- <i>N</i> -propylamine	19e	0.61	3.2	azetidine	19m	0.94	5.2
2-methoxy ethylamine	19f	>1	>10	-N(CH <sub>3</sub> ) <sub>2</sub>	1	0.3	4.4
<i>N</i> -methyl- <i>N</i> -butylamine	19g	0.69	3.2	-NHCH <sub>3</sub>	19n	0.9	>10
<i>N</i> -methyl- <i>N</i> -isopropylamine	19h	0.7	3.4	-NH <sub>2</sub>	19o	1.9	>10

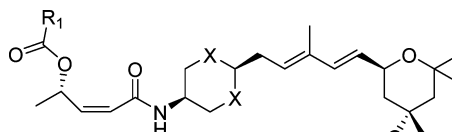
<sup>a</sup>All activities are based on the mean of three experiments after a 72 h exposure to compound. The cytotoxicity IC<sub>50</sub> values are all reported in micromolar units, with the standard error of the mean (SEM) being less than ±30% in all cases (determined as previously reported).<sup>34</sup>

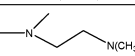
the groups used in the substitution of carbamate derivatives of these compounds. For example, although pivaloyl ester **19a** showed good activity, the *n*-butyl, diethyl, and *t*-butyl carbamates (**19b**, **19c**, and **19d**, respectively) failed to show submicromolar activity in the two cell lines used in this screen, which represents a significant reduction in activity in the cytotoxicity screen (Table 1; the SEM was less than ±30% in all cases and was determined as previously reported for the compounds in this table).<sup>34</sup> In the case of the SAR of *N,N*-dialkyl carbamates, it was noted that the presence of a *N*-methyl group was better tolerated than other groups, as can be seen with the *N*-methyl-*N*-propyl (**19e**), *N*-methyl-*N*-butyl (**19g**), and other *N*-methyl-*N*-alkyl derivatives (**19h** and **19i**) when compared to **19b** or **19c**. In addition, it is noted that cyclic carbamates (**19j–m**) showed activity near 1 μM, so no significant improvement was seen with these cyclic compounds. The most active early esterase stable compound in this series was the dimethylamino carbamate derivative **1**, which we named sudemycin F1.<sup>35</sup> On the basis of this SAR data, it could be hypothesized that a compact and relatively nonpolar pocket near (or on) the SF3B subunit interaction site exists for the ester and carbamate functionalities because activity goes down

with both the length of hydrophobic groups and with increasing polarity (Table 2), although other effects, such as cellular uptake, undoubtedly influence activity as well.

We also explored the replacement of the carbonyloxy group that is present in the active carbamates and esters with other dual hydrogen-bond-acceptor groups. If the key pharmacophore feature of the interaction of the carbonyloxy group is the presence of the dual 1,3 dihydrogen-bond acceptors, then other functional groups might also fulfill this interaction and at the same time be fully resistant to esterase metabolism. To explore this hypothesis, we prepared a set of compounds shown in Scheme 4. These heterocyclic derivatives could all be reasonable fits to the pharmacophore model if simple hydrogen-bond dual acceptors are required; however, none of these compounds showed cytotoxic IC<sub>50</sub>'s below 10 μM. This suggests that the steric requirements for this fit may be very constrained.

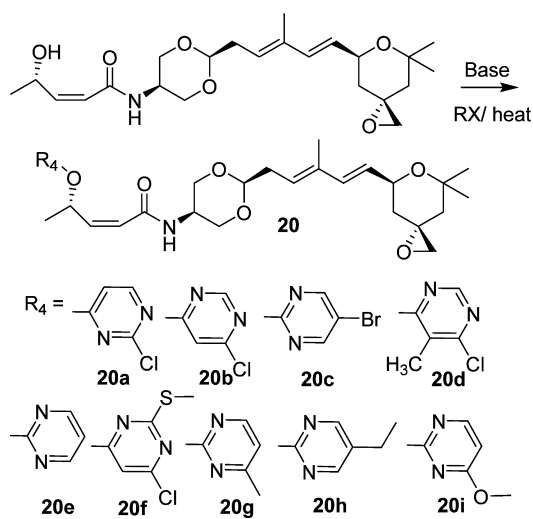
In addition, we explored the importance of the NH group in these analogues; the pharmacophore model predicted the importance of the NH hydrogen-bond donor of the amide group, and as predicted the *N*-methyl derivative of **19p** (**19q**, see the Supporting Information) showed a complete abrogation

Table 2. Comparison of the Most Active Lead Compounds<sup>a</sup>


Compound	R' =	X =	MDM2 Splicing Effects <sup>b</sup>	JeKo1 IC <sub>50</sub> nM	Plasma Stability <sup>c</sup>	Buffer Soluble <sup>d</sup>	Rapid Onset <sup>e</sup>
<b>1</b> <sup>35</sup>	-N(CH <sub>3</sub> ) <sub>2</sub>	O	> 8h	300 <sup>f</sup>	> 5 h	>10 μM	> 8 h
<b>2</b>	-N(CH <sub>3</sub> ) <sub>2</sub>	CH <sub>2</sub>	< 8h	41 <sup>g</sup>	> 5 h	<10 μM	< 8 h
<b>3</b>	-NHCH <sub>3</sub>	CH <sub>2</sub>	< 8h	22 <sup>g</sup>	> 5 h	>10 μM	< 8 h
<b>18a</b> <sup>33</sup>	-CH <sub>3</sub>	CH <sub>2</sub>	< 8h	100 <sup>f</sup>	< 5 h	<<10 μM	< 8 h
<b>18b</b> <sup>33</sup>	-CH(CH <sub>3</sub> ) <sub>2</sub>	CH <sub>2</sub>	< 8h	47 <sup>f</sup>	< 5 h	<<10 μM	< 8 h
<b>18c</b>		CH <sub>2</sub>	ND	170 <sup>f</sup>	ND	>10 μM	ND
<b>18d</b>	-NH <sub>2</sub>	CH <sub>2</sub>	ND	100 <sup>g</sup>	ND	ND	ND
<b>19p</b> <sup>34</sup>	-CH(CH <sub>3</sub> ) <sub>2</sub>	O	ND	220 <sup>g</sup>	< 5 h	>10 μM	> 8 h

<sup>a</sup>All activities are based on the mean of three experiments after a 72 h exposure to compound. The cytotoxicity IC<sub>50</sub> values are all reported in micromolar units. The standard error of the mean (SEM) for cytotoxicity values was less than ±30% in all cases and was determined as previously reported<sup>34</sup> or as described in the Experimental Section. Previously reported compounds are included for comparison and are indicated by the appropriate reference. (Protocols for all assays are provided in the Supporting Information.) ND = not determined. <sup>b</sup>Major splicing changes observed with 1 μM drug treatment of Rh18 cells. <sup>c</sup>In mouse plasma at 37 °C, as determined by HPLC. <sup>d</sup>Solubility (as determined by HPLC) in PBS. <sup>e</sup>The time to achieve the majority of the observed 72 h cytotoxicity on the basis of drug-washout experiments. <sup>f</sup>72 h cytotoxicity measured using an MTT assay, as previously reported.<sup>34</sup> <sup>g</sup>72 h cytotoxicity using a Cell Titer Glow assay, as described in the Experimental Section.

## Scheme 4. Synthesis of Heteroaryl Derivatives



of activity. These results taken together demonstrate the exquisite sensitivity of the spliceosome modulator pharmacophore, which is consistent with other published work.<sup>27,28</sup> However, despite these constraints, we were able to prepare a set of highly active compounds, as summarized in Table 2.

To explore further the SAR, we also prepared a set of exploratory compounds based on the less soluble series (containing the cyclohexyl ring rather than the 1,3-dioxane ring) to explore a set of conservative changes that could give active low-molecular-weight analogues with better solubility properties (Table 2). We were very pleasantly surprised to find that we had, for the first time, prepared compounds with improved cytotoxic activity, which also showed improved measured solubility properties. Most strikingly, carbamate **3** showed low double-digit potency in contrast to the reduced activity seen in the monomethyl carbamate derivative **19n** when compared to **1**. We then performed careful analysis of the top-

ranked lead compounds, as shown in Table 2. Compound **3** has the best profile and stands out because it possesses potent cell-based activity combined with druglike measured solubility (45 μM in PBS). Compound **3** also showed potent cytotoxic activity in several other tumor lines investigated (see the Supporting Information), including the melanoma line SK-MEL-2 (IC<sub>50</sub> = 39 nM) as well as HeLa (IC<sub>50</sub> = 50 nM), SK-N-AS (IC<sub>50</sub> = 81 nM), and PC-3 (IC<sub>50</sub> = 142 nM).

**Drug Synergy Studies.** There is increasing evidence that certain synergistic anticancer drug combinations can be both more effective and less toxic than single-agent drug protocols.<sup>42</sup> In consideration of this fact, we next turned our attention to the in vitro anticancer drug combination properties of our splicing modulators in tumor cell lines by exploration of the combined dual-agent cytotoxic effects of compounds **2** or **3** with successive members of a panel of 23 diverse types of clinically useful anticancer drugs and bioactive agents (Table 3). Although many of the combinations investigated (10 of the 23 agents) did not demonstrate either antagonism or synergy, we were able to uncover a number of drugs that show a significant combination effect in the first round of this screening efforts using the first drug panel shown in Table 3. Although the identification of antagonistic or synergistic drug combinations remains an empirical process, it is generally believed that agents that are antagonistic may both be targeting related signaling pathways and that agents that are synergistic are targeting distinct and complementary pathways.<sup>42</sup> In principle, it is also possible that an agent can also show synergy in other ways, for example, by interfering with an important drug metabolic process and therefore stabilizing an agent that is a component of the combination therapy.

Subsequent to the first screen, we focused our attention on agents showing synergy; the most notable of these was BEZ235, a dual inhibitor of phosphatidylinositol-3-kinase (PI3K) and the mammalian target of rapamycin (mTOR),<sup>43</sup> which is currently under investigation in numerous clinical trials. Given the strong synergy that we observed with BEZ235,

**Table 3. Drug Combinations<sup>a</sup> Showing Antagonism or Synergy of Cytotoxicity of SK-MEL-2 with Compound 2<sup>b</sup>**

first drug panel			
drug	mechanism of action	interaction type	CI in SK-MEL-2
BEZ235	dual inhibitor of PI3K and mTOR	strong synergism	0.21
bortezomib	proteasome inhibitor	antagonism	n.d. <sup>c</sup>
camptothecin	DNA topoisomerase I inhibitor	moderate synergism	0.74
harringtonine	inhibitor of protein synthesis	antagonism	n.d.
imatinib	tyrosine kinase inhibitor	antagonism	n.d.
panobinostat	broad-spectrum HDAC inhibitor	moderate synergism	0.76
silibinin	multiple Targets	slight synergism	0.89
sorafenib	multikinase inhibitor (inhibits sEH)	synergism	0.43
SU 9516	cyclin-dependent kinase-2 inhibitor	moderate synergism	0.83
taxol	microtubule inhibitor	antagonism	n.d.
follow-up drug panel			
drug	mechanism of action	interaction type	CI in SK-MEL-2
PX-866	irreversible inhibitor of PI3K	synergism	0.57
temsirolimus	inhibitor of mTORC1	synergism	0.68
AUDA	inhibitor of sEH	synergism	n.d.

<sup>a</sup>For the complete table including the full list of drugs that were tested, see Supporting Information Tables 2 and 3. <sup>b</sup>See the Supporting Information for combination indexes for each drug combination investigated. <sup>c</sup>The notation n.d. indicates that the CI value was not determined. For some compounds such as AUDA, it is not possible to determine a CI because AUDA does not show cytotoxicity as a single agent. Drug interaction was established by combination of various concentrations of compound 2 combined with the indicated drug at a constant concentration.

we decided to investigate the combined effects of selective inhibitors of the two individual targets (i.e., PI3K and mTOR).<sup>44</sup> For this we chose PX-866 and temsirolimus, which are selective inhibitors of PI3K and mTOR, respectively. Interestingly, both of these agents showed synergy with lead compound 2, although not as strong as that observed with the dual-acting agent BEZ235 (Table 3, follow-up drug panel). As evident in Figure 3, this synergy is also seen with our best lead for both 2 and 3 in all cell lines investigated. The second strongest synergistic agent in the first drug panel was the multikinase inhibitor sorafenib, which is also reported to have off-target inhibition of soluble epoxide hydrolase (sEH).<sup>45</sup> Some mammalian epoxide hydrolases are known to be important in the metabolism of epoxide-containing xenobiotics.<sup>46</sup> Because the sudemycins (and related drugs) have an epoxide group as a critical feature of their pharmacophore,<sup>33</sup> it is possible that this group is metabolized and inactivated by epoxide hydrolases present in tumor cells during the course of the cytotoxicity screening. We prepared the diol product of epoxide ring-opening of compound 3 and found that this compound showed no detectable activity at a concentration of 10  $\mu$ M (see the Supporting Information, Scheme S4 and associated experimental procedures). Therefore, we hypothesized that EH inhibitors may stabilize this class of drugs, so we explored the use of the EH inhibitor AUDA. As shown in Table 3, AUDA also demonstrates synergy with compound 2,

supporting the possibility that this epoxide metabolic pathway is significant for these drugs in vitro and potentially in vivo. It should be noted that because agents such as AUDA do not show cytotoxic effects the combination index (CI) can not be calculated for them. Of course, these drug-synergy studies are relevant for the design of potential future clinical studies that would include the use of relevant drug combinations of sudemycin D6.

**In Vivo Tumor Xenograft Studies.** Previously, our group reported the in vivo efficacy of the early lead sudemycin C1,<sup>35</sup> which inhibited tumor growth in a lymphoma xenograft model when delivered intravenously.<sup>34</sup> Although the sudemycin C1-treated mice showed significant inhibition of tumor growth in this model (when compared to that of the vehicle-treated group), tumor proliferation was not completely inhibited. It is likely that the incomplete inhibition seen in our earlier study was a consequence of the short in vivo half-life of sudemycin C1. We propose that the observed short half-life is due to the presence of a labile ester group that is present in sudemycin C1, which we have previously shown.<sup>34</sup> It is well-known that esters are substrates for plasma and microsomal esterases that can rapidly metabolize esters to the corresponding alcohols, and this topic has recently been reviewed.<sup>48</sup> We have previously reported that hydrolysis of sudemycin C1 leads to an inactive alcohol (see the Supporting Information for the assay protocol).<sup>34</sup> The other metabolically labile group that is required for activity in the sudemycins and the natural products<sup>27</sup> is the epoxide group, which can be a target for epoxide hydrolases, which would produce the inactivated diol metabolites.<sup>46</sup> This led us to conclude that it was necessary to deliver the drug via slow continuous jugular catheter (JVC) infusion in our in vivo efficacy studies.

Thus, following maximum tolerated dose (MTD) (data not shown) and pharmacokinetic studies (see the Supporting Information, in vivo pharmacokinetic studies), we sought to determine the efficacy of lead compound 3 in the inhibition of tumor growth in mice (Figure 4). Thus, SK-MEL-2 tumors were transplanted into male C.B-17 scid mice. The animals were subsequently infused over 4 h with either vehicle (eight mice) or compound 3 (nine mice) for 5 consecutive days. No differences in fatalities or behavioral changes were observed between the control infusion and the drug-treatment groups. In the drug-treated group (50 mg/kg of compound 3 over 4 h once a day for 5 days) (Figure 4), we observed 100% inhibition of tumor growth during the infusion period and significant inhibition subsequent to this dosing period. When compound 3 was infused over a period of 4 h, it also induced moderate toxicity (as measured by weight loss); we observed an average maximum loss of weight of  $12.7 \pm 2.3\%$  at 5 days of treatment. Nevertheless, the drug-treated group regained weight immediately after the cessation of the drug infusion, and the animals returned to a normal weight range compared to the vehicle-infused mice by day 22 of the study. This demonstrates the single-agent antitumor effects of splicing modulator 3 in this xenograft model of an aggressive metastatic human melanoma.

## CONCLUSIONS

The regulation of the pre-mRNA splicing process is abnormal in most cancers, and numerous spliceosomal proteins are known to be recurrently mutated in a variety of tumors. We have optimized a class of totally synthetic natural-product analogues targeting the spliceosome, leading to sudemycin D6 (compound 3), and further explored the SAR of this series.

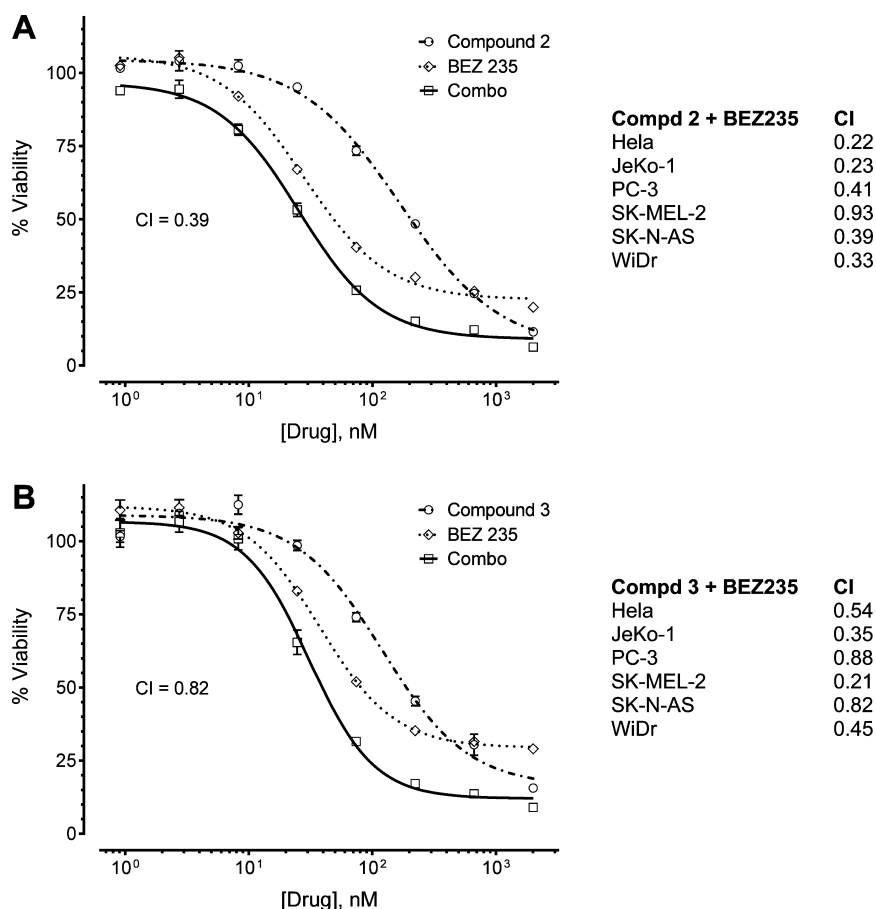


**Figure 3.** Interactions between (A) compound 2 and BEZ 235 and (B) compound 3 and BEZ 235 result in strong synergism. The  $IC_{50}$  curves of drug combinations in the neuroblastoma cell line SK-N-A-S are plotted. The combination indexes (CI) shown to the right were calculated at the concentration of drugs required to inhibit 50% of cell proliferation ( $ED_{50}$ ) in various cell lines. Each experimental condition was carried out in triplicate; error bars represent the SEM. Drug interactions were assessed with CalcuSyn 2.1 (Biosoft, Cambridge, UK). The program is based on Chou–Talalay’s combination index theorem, which renders a quantitative definition of the drugs’ interaction defined as the CI.<sup>47</sup>

Sudemycin D6 shows potent cytotoxic activity in the melanoma line SK-MEL-2 ( $IC_{50}$  = 39 nM) as well as several other tumor lines that were investigated, including JeKo-1 ( $IC_{50}$  = 26 nM), HeLa ( $IC_{50}$  = 50 nM), SK-N-AS ( $IC_{50}$  = 81 nM), and PC-3 ( $IC_{50}$  = 142 nM). Sudemycin D6 also shows rapid and potent modulation of MDM2 alternate splicing in the Rh18 cell line as well as acceptable plasma stability, which led to its selection for in vivo studies. These in vivo studies demonstrate the activity of sudemycin D6 in a mouse melanoma xenograft model. In addition to this work, we also report improved synthetic processes for this class of compounds (including 2 and 3) as well as data from in vitro drug-synergy studies using a panel of anticancer drugs. This work supports the idea that sudemycin D6 is worthy of further investigation as a novel preclinical anticancer agent, which may have application in the treatment of several types of human cancers.

## EXPERIMENTAL SECTION

**Biology General Aspects. Cell Culture.** Cancer cell lines were purchased from the American Type Culture Collection (Manassas, VA) with the exception of the pediatric rhabdomyosarcoma Rh18, which was kindly provided by Dr. P. Houghton (Ohio State University, Nationwide Children’s Hospital, Columbus, OH). The following cell media was used: JeKo-1 (mantle cell lymphoma) cells were grown in RPMI 1640 medium containing 20% fetal bovine serum (FBS); PC-3 (prostate adenocarcinoma) cells were grown in Ham’s F-12K with 10% FBS; HeLa (cervical adenocarcinoma), SK-MEL-2

(malignant melanoma), and WiDr (colorectal adenocarcinoma) cells were grown in EMEM medium containing 10% FBS; and neuroblastoma SK-N-AS cells were grown in RPMI 1640 medium containing 10% FBS. All cell culture media was supplemented with L-glutamine and penicillin/streptomycin. All cells were grown under standard conditions in  $CO_2$  incubators at 37 °C with 5%  $CO_2$  and 100% relative humidity.

**In Vitro Cytotoxicity Assays.** The concentration of drug required to inhibit cell proliferation by 50% ( $IC_{50}$ ) was determined as the percentage of viable cells remaining after a 72 h exposure to the drug. Adherent cells were seeded in 100  $\mu$ L of cell culture medium in 96-well plates. Depending on the cell proliferation rate, cells were seeded at 4000–6000 cells/well. Suspension cell cultures were initiated with 20 000 cells/well. The cells were incubated overnight at 37 °C, and then the drug treatments were started by adding 50  $\mu$ L of medium containing the corresponding drug dilution and DMSO. The final concentration of DMSO onto the cells was 0.5% v/v in all wells. Cell viability was determined using the CellTiter-Glo Luminescent Cell Viability Assay (Promega, Madison, WI). The CellTiter-Glo reagent was prepared according to the manufacturer’s instructions, and then 50  $\mu$ L of reagent was added to each well for 1 h at rt. The luminescence was measured on an EnVision Multilabel Plate Reader (PerkinElmer, Waltham, MA). The  $IC_{50}$  values were calculated from the dose–response curve analysis with GraphPad Prism 6.01 (GraphPad Software, La Jolla, CA) using the nonlinear regression model 4 parameter logistic. Nine concentrations were generated by 1:2 serial dilutions for each  $IC_{50}$  assay. Each drug concentration was evaluated in triplicate or quadruplicate.

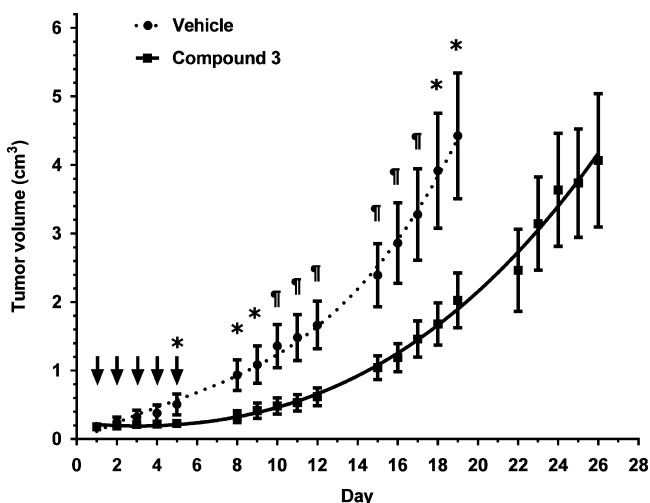


**Figure 4.** Compound 3 inhibits SK-MEL-2 tumor growth in a mouse xenograft model. The arrows indicate a 4 h infusion of 50 mg/kg of either vehicle or compound 3. Tumor growth was monitored daily five times per week.  $n = 8$  for the vehicle group and 9 for the drug-treated group. Mice were euthanized when the tumor burden reached the size limit ( $>4 \text{ cm}^3$ ). Error bars represent the SEM. Statistical evaluations were assessed using one-tailed Student's  $t$ -test, and the symbols above the lines indicate significant differences at  $* = p < 0.05$  and  $\parallel = p < 0.01$ .

**Drug Combination Assays.** Preliminary cytotoxic screenings for each drug used in drug combination assays were performed to determine their cytotoxic dose range. The drug combination assays were initiated at a dose that was 4 or more times higher than the concentration of each drug required for the  $\text{IC}_{50}$  value. Eight concentrations were established by 1:3 serial dilutions of the single drugs and their combinations with the splicing modulators. All drug concentrations were evaluated in triplicate in 96-well cell culture plates. Assays of individual drugs and drug combinations were run on the same cell culture plate. Cell viability was determined using the CellTiter-Glo reagent. Drug interactions, in terms of synergism, additive effect, or antagonism, were based on the drugs' CI.<sup>47</sup>

**Combination Index for Constant-Ratio Drug Combinations.** Luminescence data obtained from the cell viability determinations were formatted per the requirements of the analytical software (viability data range  $>0$  and  $<1$ ). The formatted data were analyzed with CalcuSyn 2.1 (Biosoft, Cambridge, UK), which provides quantitative CI values for the drug-interaction analyses (see ranges in Supporting Information Table S2). All CI values were calculated at the combination dose that produced a cytotoxic effect in 50% of the cells ( $\text{ED}_{50}$ ). AUDA does not show any cytotoxicity at any achievable concentration, so it was not possible to determine a CI for those drugs. Therefore, in these two cases, the drug interaction was evaluated by comparing the  $\text{IC}_{50}$  value of sudemycin standard (D1 or D6) with that of the  $\text{IC}_{50}$  values resulting from the serial dilutions of the splicing modulator combined with a constant dose of the nontoxic drug.

**Infusions in Tumor-Bearing Mice.** Xenograft tumors were first established from an SK-MEL-2 cell culture at the St. Jude Children's Research Hospital Xenograft Core. After these tumors were established as a mouse xenograft model, they were routinely maintained in the C.B-17 scid strain (Taconic Farms, Germantown, NY). Experimental animals were prepared by transplanting small pieces of dissected tumors from donor animals into recipient mice. All animal studies were performed in accordance with the St. Jude Children's Research Hospital Animal Care and Use Committee. SK-MEL-2 xenograft tumors were transplanted into male C.B-17 scid mice on day  $-21$ . On days  $-7$  to  $-5$ , a jugular vein catheter was surgically implanted into each mouse. Beginning on day 1, the animals (eight for vehicle and nine for drug treatment) received daily infusions of vehicle (10% 2-hydroxypropyl- $\beta$ -cyclodextrin dissolved in 50 mM  $\text{Na}_2\text{HPO}_4$ /

$\text{NaH}_2\text{PO}_4$ , pH 7.4) or 50 mg/kg of lead compound 3 for 5 consecutive days. Infusions were carried out by placing the animals inside a continuous infusion system (Instech Laboratories, Plymouth Meeting, PA) and delivering the vehicle or drug solution via the jugular catheter at a rate of  $4 \mu\text{L}/\text{min}$  with a SP230iw syringe pump (WPI, Sarasota, FL). The total volume infused into the animals did not exceed  $850 \mu\text{L}$  per day. Tumor size and animal weight were both continuously measured during and after infusion periods, five times per week (weekdays). Tumor volumes were determined on the basis of the following equation:  $\text{Tu}_{\text{vol}} = (\delta_1/2 + \delta_2/2)^{1.5708}$ , where  $\delta_1$  and  $\delta_2$  are diameters measured with a caliper at right angles to each other. The size of the tumors ranged from 0.2 to  $0.5 \text{ cm}^3$  at the times the infusions were initiated.

**Chemistry General Aspects.** All materials and reagents were used as is unless otherwise indicated. Air- or moisture-sensitive reactions were carried out under a nitrogen atmosphere. THF, toluene, acetonitrile,  $N,N$ -dimethyl formamide, and  $\text{CH}_2\text{Cl}_2$  were distilled before use. All compounds were purified on Biotage prepacked silica gel columns. TLC analysis was performed using glass TLC plates (0.25 mm, 60 F-254 silica gel). Visualization of the developed plates was accomplished by staining with ethanolic phosphomolybdic acid, ceric ammonium molybdate, or ethanolic ninhydrin followed by heating on a hot plate ( $120 \text{ }^\circ\text{C}$ ). All compounds for biological assays possessed a purity of  $>95\%$  as determined by ultra-high-pressure liquid chromatography on a Waters Acquity UPLC/PDA/ELSD/MS system carried out with a BEH C18  $2.1 \times 50 \text{ mm}$  column using gradient elution with stationary phase: BEH C18, 1.7 mm, solvents: A: 0.1% formic acid in water, B: 0.1% formic acid in acetonitrile. NMR spectra were obtained on Bruker Avance II 400 MHz. The values  $d_{\text{H}}$  7.26 and  $d_{\text{C}}$  77.0 ppm were used as references for NMR spectroscopy in  $\text{CDCl}_3$ . The coupling constants deduced from  $^1\text{H}$  NMR data were obtained by first-order coupling analysis. Analytical and/or preparative SFC (supercritical fluid chromatography) systems (AD-H) were used for analysis and purification of final chiral compounds. IR spectra were collected using a Nicolet IR 100 (FT IR). FT IR analyses were prepared neat or as neat films on KBr plates, and the data are reported in wavenumbers ( $\text{cm}^{-1}$ ) unless specified otherwise. Melting points (mp) were obtained on a Buchi apparatus and are uncorrected. The University of Illinois Mass Spectroscopy Laboratories and High Throughput Analytical Center at St. Jude Children's Research Hospital collected the high-resolution mass spectral data.

**Chemistry Procedures.** *(S,Z)-5-(((2R,5R)-2-((2E,4E)-5-((3R,5S)-7,7-dimethyl-1,6-dioxaspiro[2.5]octan-5-yl)-3-methylpenta-2,4-dien-1-yl)-1,3-dioxan-5-yl)amino)-5-oxopent-3-en-2-yl Dimethylcarbamate (1).* A stirred solution of *(S,Z)-5-(((2R,5R)-2-((2E,4E)-5-((3R,5S)-7,7-dimethyl-1,6-dioxaspiro[2.5]octan-5-yl)-3-methylpenta-2,4-dien-1-yl)-1,3-dioxan-5-yl)amino)-5-oxopent-3-en-2-yl (4-nitrophenyl) carbonate* (2.4 g, 4.09 mmol) in dichloroethane (35 mL) in an ice bath was treated with dimethylamine (6.14 mL, 12.27 mmol, 2 M in THF) dropwise. The resulting yellow solution was stirred at the same temperature for 10 min, by which time LC/MS indicated that all starting material had been consumed. The solvent was then removed under reduced pressure. The yellow viscous crude residue was dissolved in a minimum volume of methylene chloride and treated with hexane. The resulting yellow solids were filtered and washed with 5% methylene chloride in hexane (25 mL). The filtrate was concentrated and purified on silica gel (100 g, 8–70% acetone in hexane) to give 1.72 g (86%) of carbamate as a fluffy solid.  $^1\text{H}$  NMR (400 MHz,  $\text{CDCl}_3$ )  $\delta$  7.93 (d,  $J = 8.2 \text{ Hz}$ , 1H), 6.27 (d,  $J = 15.8 \text{ Hz}$ , 1H), 5.91–5.84 (m, 1H), 5.84–5.78 (m, 2H), 5.58 (dd,  $J = 15.7$ , 6.6 Hz, 1H), 5.50 (t,  $J = 7.2 \text{ Hz}$ , 1H), 4.58 (t,  $J = 5.3 \text{ Hz}$ , 1H), 4.45 (ddd,  $J = 11.0$ , 6.6, 1.8 Hz, 1H), 4.06–3.87 (m, 5H), 2.89 (s, 6H), 2.58–2.54 (m, 2H), 2.54–2.47 (m, 2H), 2.03–1.86 (m, 2H), 1.73 (d,  $J = 0.9 \text{ Hz}$ , 3H), 1.41–1.35 (m, 6H), 1.27 (s, 3H), 1.24–1.11 (m, 2H).  $^{13}\text{C}$  NMR (101 MHz,  $\text{CDCl}_3$ )  $\delta$  165.23, 156.30, 141.45, 135.70, 135.48, 127.86, 125.92, 123.67, 102.04, 73.04, 70.15, 70.12, 69.50, 69.39, 55.66, 51.05, 43.80, 42.45, 38.59, 36.31, 35.90, 34.20, 31.54, 23.77, 20.44, 12.59. HRMS (ESI)  $m/z$  calcd for  $\text{C}_{26}\text{H}_{40}\text{N}_2\text{O}_7\text{Na}$  ( $\text{M} + \text{Na}$ )<sup>+</sup>, 515.2733; found, 515.2734.

(*S,Z*)-5-(((1*R*,4*R*)-4-((2*E*,4*E*)-5-((3*R*,5*S*)-7,7-Dimethyl-1,6-dioxaspiro[2.5]octan-5-yl)-3-methylpenta-2,4-dien-1-yl)cyclohexylamino)-5-oxopent-3-en-2-yl Dimethylcarbamate (**2**). A solution of activated carbonate **17** (1 g, 1.7 mmol) in dichloroethane (15 mL) at 0 °C was treated with dimethylamine (2.57 mL, 5.15 mmol, 2 M in THF) dropwise. The resulting yellow solution was allowed to stir at 0 °C for 10 min, by which time the TLC indicated that all of the starting material had been consumed. The solids formed (*p*-nitro phenol) in the reaction were filtered and washed with 5% methylene chloride in hexane (2 × 15 mL). The filtrate was concentrated, and the resulting residue was purified on silica column (10–80% EtOAc in hexane) to give 755 mg (90%) of dimethyl carbamate derivative **2** as a fluffy solid. <sup>1</sup>H NMR (400 MHz, CDCl<sub>3</sub>) δ 8.23 (d, *J* = 8.0 Hz, 1H), 6.27 (d, *J* = 15.6 Hz, 1H), 5.82 (d, *J* = 11.4 Hz, 1H), 5.64–5.46 (m, 4H), 4.51–4.39 (m, 1H), 4.18–4.06 (m, 1H), 2.91 (s, 6H), 2.57 (s, 2H), 2.14–2.04 (td, *J* = 7.0, 4.6 Hz, 2H), 2.04–1.85 (m, 3H), 1.75–1.65 (m, 2H), 1.71 (s, 3H), 1.63–1.51 (m, 4H), 1.42–1.32 (s, 2H), 1.39 (s, 3H), 1.34 (d, *J* = 6.1 Hz, 3H), 1.28 (s, 3H), 1.24–1.10 (m, 2H). <sup>13</sup>C NMR (101 MHz, CDCl<sub>3</sub>) δ 165.15, 156.45, 136.36, 136.27, 133.60, 132.30, 126.85, 126.27, 73.02, 69.61, 69.53, 55.67, 51.03, 45.24, 42.45, 38.63, 36.66, 36.26, 35.89, 34.55, 31.53, 29.64, 29.50, 27.76, 27.43, 23.76, 20.66, 12.44. IR (neat film) 3267, 2874, 2804, 1656, 1635, 1511, 1370, 1172, 1038 cm<sup>-1</sup>. HRMS (ESI) *m/z* calcd for C<sub>28</sub>H<sub>43</sub>N<sub>2</sub>O<sub>5</sub> (M + H)<sup>+</sup>, 489.3323; found, 489.3334.

(*S,Z*)-5-(((1*R*,4*R*)-4-((2*E*,4*E*)-5-((3*R*,5*S*)-7,7-Dimethyl-1,6-dioxaspiro[2.5]octan-5-yl)-3-methylpenta-2,4-dien-1-yl)cyclohexylamino)-5-oxopent-3-en-2-yl Methylcarbamate (**3**). A stirred solution of activated carbonate **17** (100 mg, 0.17 mmol) in 1,2-dichloroethane (0.3 mL) was cooled in an ice bath and slowly treated with methylamine (77 μL, 0.51 mmol, 2 M in THF). The resulting yellow solution was stirred at 0 °C for 10 min. The solid precipitate (*p*-nitro phenol) was removed by filtration, and the residue was washed with a mixture of methylene chloride and hexane. The combined filtrates were concentrated, and the residue was purified on a silica column (25g, 15–100% EtOAc in hexane) to give 75 mg (92%) of methyl carbamate **3** as a white viscous solid. <sup>1</sup>H NMR (400 MHz, CDCl<sub>3</sub>) δ 7.94 (d, *J* = 7.7 Hz, 1H), 6.26 (d, *J* = 15.7 Hz, 1H), 5.82 (d, *J* = 10.8 Hz, 1H), 5.66–5.44 (m, 4H), 4.77 (s, 1H), 4.52–4.39 (m, 1H), 4.18–4.06 (m, 1H), 2.78 (d, *J* = 5.0 Hz, 3H), 2.57 (s, 2H), 2.09 (t, *J* = 7.1 Hz, 2H), 2.05–1.87 (m, 2H), 1.80–1.67 (m, 2H), 1.72 (s, 3H), 1.65–1.49 (m, 4H), 1.48–1.41 (m, 1H), 1.40 (s, 3H), 1.38–1.34 (m, 2H), 1.31 (d, *J* = 5.8 Hz, 3H), 1.28 (s, 3H), 1.24–1.12 (m, 2H). <sup>13</sup>C NMR (101 MHz, CDCl<sub>3</sub>) δ 165.17, 157.03, 136.66, 136.16, 133.70, 132.10, 126.80, 126.06, 73.06, 69.52, 69.15, 55.68, 51.04, 45.36, 42.46, 38.57, 36.62, 34.42, 31.52, 29.57, 29.44, 27.68, 27.39, 27.33, 23.76, 20.60, 12.44. HRMS (ESI) *m/z* calcd for C<sub>27</sub>H<sub>43</sub>N<sub>2</sub>O<sub>5</sub> (M + H)<sup>+</sup>, 475.3172; found, 475.3188.

2-(((3*R*,5*S*)-7,7-Dimethyl-1,6-dioxaspiro[2.5]octan-5-yl)methylsulfonyl)benzo[d]thiazole (**5**). A stirred solution of sulfide **9** (29 g, 90 mmol) in EtOH (700 mL) was cooled in an ice bath and treated with a mixture of ammonium molybdate·4H<sub>2</sub>O (33.4 g, 27 mmol) and 30% H<sub>2</sub>O<sub>2</sub> (123 mL, 1.08 mol) that had been adjusted to pH 4 to 5 with 7.0 phosphate buffer (49 mL, 0.26 M) at 0 °C before the addition. The resulting suspension was allowed to stir for 14 h at rt. The reaction solution was divided into two portions for further workup. Each portion was diluted with water (400 mL), and CH<sub>2</sub>Cl<sub>2</sub> (400 mL) and the aqueous layer were extracted with CH<sub>2</sub>Cl<sub>2</sub> (2 × 300 mL) and washed with brine (1 × 300 mL). The two organic portions were combined and dried over Na<sub>2</sub>SO<sub>4</sub>. The solvent was evaporated under reduced pressure to give the crude product as a white viscous solid. This was crystallized using methylene chloride and hexane to give 29 g (91%) of pure sulfone **5** as a white solid. mp 124–126 °C. [α]<sub>D</sub><sup>24</sup> +4.5° (c 1.1, CHCl<sub>3</sub>). <sup>1</sup>H NMR (400 MHz, CDCl<sub>3</sub>) δ 8.25–8.17 (m, 1H), 8.04–7.97 (m, 1H), 7.67–7.52 (m, 2H), 4.62–4.54 (m, 1H), 3.91 (dd, *J* = 14.8, 9.2 Hz, 1H), 3.43 (dd, *J* = 14.7, 2.8 Hz, 1H), 2.53 (dd, *J* = 17.9, 4.5 Hz, 2H), 1.96–1.74 (m, 2H), 1.25 (s, 3H), 1.23–1.20 (m, 1H), 1.01 (dd, *J* = 14.0, 1.8 Hz, 1H), 0.59 (s, 3H). <sup>13</sup>C NMR (101 MHz, CDCl<sub>3</sub>) δ 166.96, 152.69, 136.85, 127.80, 127.43, 125.40, 122.16, 73.53, 64.03, 60.14, 54.92, 50.80, 42.02, 37.02, 30.27, 22.90. IR (neat film) 2973, 2916, 1475, 1423, 1325, 1147, 1088, 1027 cm<sup>-1</sup>.

HRMS (ESI) *m/z* calcd for C<sub>16</sub>H<sub>20</sub>NO<sub>4</sub>S<sub>2</sub> (M + H)<sup>+</sup>, 354.0834; found, 354.0843.

2-(((3*R*,5*S*)-7,7-Dimethyl-1,6-dioxaspiro[2.5]octan-5-yl)methylthio)benzo[d]thiazole (**9**). A solution of alcohol **8** (19.5 g, 113 mmol) in THF (750 mL) was treated with Ph<sub>3</sub>P (32.7 g, 6.31 mmol) and 2-mercapto benzothiazole (20.5 g, 119 mmol) and allowed to stir at rt. After 15 min, the reaction solution was cooled to 0 °C as a solution of diisopropyl azodicarboxylate (26 mL, 125 mmol) in toluene (70 mL) was added dropwise. The resulting yellow suspension was allowed to stir for 1 h at 0 °C. The reaction mixture was then concentrated, and the residue was triturated with 10% EtOAc in hexane (500 mL). The solids were filtered and washed with 7.5% EtOAc in hexane (3 × 100 mL). The filtrate was then evaporated, and the resulting residue was purified by flash chromatography (750 g, 5–30% EtOAc in hexane) to give 27.6 g (76%) of sulfide derivative **9** as a viscous oil. [α]<sub>D</sub><sup>24</sup> +49.9° (c 1.3, CHCl<sub>3</sub>). <sup>1</sup>H NMR (400 MHz, CDCl<sub>3</sub>) δ 7.87–7.82 (m, 1H), 7.76–7.72 (m, 1H), 7.44–7.37 (m, 1H), 7.32–7.27 (m, 1H), 4.35–4.24 (m, 1H), 3.54 (ddd, *J* = 19.8, 13.2, 5.8 Hz, 2H), 2.57 (q, *J* = 4.6 Hz, 2H), 2.03–1.92 (m, 2H), 1.42–1.34 (m, 4H), 1.25 (s, 3H), 1.16 (dd, *J* = 13.9, 1.9 Hz, 1H). <sup>13</sup>C NMR (101 MHz, CDCl<sub>3</sub>) δ 167.14, 153.17, 135.33, 125.98, 124.16, 121.46, 120.95, 73.58, 67.46, 55.56, 50.94, 42.42, 38.76, 37.04, 31.26, 23.72. IR (neat film) 2973, 2910, 1459, 1428, 1252, 1090, 1055, 1020 cm<sup>-1</sup>. HRMS (ESI) *m/z* calcd for C<sub>16</sub>H<sub>20</sub>NO<sub>2</sub>S<sub>2</sub> (M + H)<sup>+</sup>, 322.0935; found, 322.0930.

2-(((1*S*,4*S*)-4-Azidocyclohexyl)ethanol (**11**). A stirred solution of alcohol **10** (10 g, 41.1 mmol) in methylene chloride (160 mL) was cooled in an ice bath as trifluoroacetic acid (35.1 mL, 431 mmol) was slowly added. The resulting solution was allowed to warm to rt and stirred for an additional 4 h. The solvent was then evaporated under reduced pressure, and the resulting residue was dissolved in MeOH (200 mL), cooled in an ice bath, and then treated with solid K<sub>2</sub>CO<sub>3</sub> (17.0 g, 123 mmol). This mixture was allowed to stir for 1 h, filtered through a sintered funnel, and washed with methylene chloride (2 × 50 mL). The combined filtrates were concentrated to give the free amine (5.8 g) as an oil. The crude amine was used in the next step without further purification.

A stirred solution of amine derivative (5.8 g, 40.5 mmol) in MeOH (225 mL) was sequentially treated with K<sub>2</sub>CO<sub>3</sub> (12.5 g, 91 mmol) and CuSO<sub>4</sub>·5H<sub>2</sub>O (0.1 g, 0.4 mmol). The mixture was cooled in an ice bath and 1*H*-imidazole-1-sulfonylazide HCl [CAUTION: Subsequent to our development of this procedure, this reagent (as the HCl salt) was shown to be an explosion hazard, and safe alternatives have been discovered, which include the hydrogen sulfate salt. Because of this, we do not recommend that the HCl salt be used in the future]<sup>41,49</sup> (9.4 g, 54.7 mmol) was added portionwise to the resulting suspension. The reaction was warmed to rt and stirred overnight. The reaction mixture was then concentrated under vacuum and diluted with water (100 mL). The product was extracted with EtOAc (2 × 250 mL), and the combined organic layers were dried over Na<sub>2</sub>SO<sub>4</sub>. This was concentrated, and the resulting residue was purified on a silica column (160 g, 6–40% acetone in hexane) to give 5 g (73%) of the azide derivative **11** as a colorless oil. <sup>1</sup>H NMR (400 MHz, CDCl<sub>3</sub>) δ 3.84–3.74 (m, 1H), 3.69 (t, *J* = 6.1 Hz, 2H), 1.88–1.72 (m, 2H), 1.66–1.43 (m, 8H), 1.40–1.18 (m, 2H). <sup>13</sup>C NMR (101 MHz, CDCl<sub>3</sub>) δ 60.57, 57.92, 39.01, 32.67, 29.14, 27.45. IR (neat film) 3274, 2872, 2802, 2061, 1419, 1236, 1032 cm<sup>-1</sup>. HRMS (ESI) *m/z* calcd for C<sub>8</sub>H<sub>16</sub>N<sub>3</sub>O (M + H)<sup>+</sup>, 170.1288; found, 170.1281.

(*E*)-Ethyl 4-(((1*S*,4*S*)-4-Azidocyclohexyl)-2-methylbut-2-enoate (**12**). A cold (–78 °C) stirred solution of oxalyl chloride (20.6 mL, 2 M in methylene chloride, 41.4 mmol) in anhydrous methylene chloride (80 mL) was treated with DMSO (4.2 mL, 59.1 mmol) dropwise. The resulting mixture was stirred for 15 min at –78 °C and treated with a solution of alcohol **11** (5 g, 29.5 mmol) in methylene chloride (60 mL). The resulting slurry was allowed to stir at –78 °C for 60 min and then treated with diisopropylethylamine (26.3 mL, 148 mmol). The cooling bath was removed, and the reaction mixture was allowed to stir at rt for 1 h to afford a yellow solution. This solution was then cooled in an ice bath and then treated with ethyl 2-(triphenylphosphoranylidene)propanoate (16.0 g, 44.3 mmol) with stirring for 10 min. The resulting stirred suspension was then allowed

to warm to rt and allowed to stir overnight. Water (100 mL) and ether (300 mL) were then added to the reaction mixture. The organic layer was separated and washed sequentially with water (100 mL) and brine (50 mL) and dried over Na<sub>2</sub>SO<sub>4</sub>. This was concentrated, and the resulting residue was purified on a silica column (160 g, 2–20% EtOAc in hexane) to give 7 g (94%) of conjugated ester **12** as an oil. <sup>1</sup>H NMR (400 MHz, CDCl<sub>3</sub>) δ 6.75 (tq, *J* = 7.7, 1.5 Hz, 1H), 4.29–4.14 (q, *J* = 7.1 Hz, 2H), 3.86–3.72 (m, 1H), 2.11 (t, *J* = 7.5 Hz, 2H), 1.87–1.76 (m, 5H), 1.62–1.48 (m, 5H), 1.35–1.30 (m, 2H), 1.31 (t, *J* = 7.1 Hz, 3H). <sup>13</sup>C NMR (101 MHz, CDCl<sub>3</sub>) δ 168.19, 140.43, 128.69, 60.45, 57.70, 36.43, 35.39, 29.22, 27.40, 14.30, 12.54. IR (neat film) 2874, 2804, 2061, 1677, 1236 cm<sup>-1</sup>. HRMS (ESI) *m/z* calcd for C<sub>13</sub>H<sub>20</sub>N<sub>3</sub>O<sub>2</sub> (M – H)<sup>+</sup>, 250.1707; found, 250.1716.

(*E*)-4-((1*S*,4*S*)-4-Azidocyclohexyl)-2-methylbut-2-en-1-ol (**13**). A solution of diisobutylaluminum hydride (66 mL, 1.0 M in hexanes) was added dropwise to a cold (–78 °C) stirred solution of ester **12** in methylene chloride (150 mL). The resulting mixture was allowed to stir at –78 °C for 2.5 h. The reaction was quenched with MeOH (9 mL) and diluted with saturated sodium potassium tartrate tetrahydrate (150 mL) and EtOAc (160 mL). The resulting mixture was then allowed to stir vigorously for 2 h at rt to obtain a clear solution. The aqueous layer was extracted with EtOAc (2 × 200 mL), and the combined organic layers were dried over Na<sub>2</sub>SO<sub>4</sub>. This was concentrated, and the residue was purified on a silica column (160 g, 5–40% EtOAc in hexane) to give 5.3 g (91%) of pure alcohol **13** as an oil. <sup>1</sup>H NMR (400 MHz, CDCl<sub>3</sub>) δ 5.41 (t, *J* = 7.2 Hz, 1H), 4.01 (s, 2H), 3.83–3.73 (m, 1H), 1.97 (t, *J* = 6.9 Hz, 2H), 1.85–1.75 (m, 4.3 Hz, 2H), 1.66 (s, 3H), 1.60–1.48 (m, 2H), 1.41–1.23 (m, 4H). <sup>13</sup>C NMR (101 MHz, CDCl<sub>3</sub>) δ 135.69, 124.36, 68.96, 57.95, 36.85, 29.25, 27.32, 13.85. IR (neat film) 3275, 2870, 2801, 2060, 1418, 1236, 993 cm<sup>-1</sup>. HRMS (ESI) *m/z* calcd for C<sub>11</sub>H<sub>19</sub>N<sub>3</sub>ONa (M + Na)<sup>+</sup>, 232.1426; found, 232.1423.

(*E*)-4-((1*S*,4*S*)-4-Azidocyclohexyl)-2-methylbut-2-enal (**14**). A solution of alcohol **13** (3.3 g, 15.7 mmol) and pyridine (12 mL) in anhydrous methylene chloride (80 mL) at 0 °C was treated with Dess–Martin periodinate (12.4 g, 23.6 mmol) portionwise. The resulting solution was stirred for 2 h at rt and added to a 1:1 mixture (300 mL) of a saturated aqueous NaHCO<sub>3</sub> solution and saturated aqueous sodium thiosulfate solution. This mixture was allowed to stir for 30 min at rt. The aqueous layer was separated and extracted with EtOAc (2 × 400 mL), and the combined organic fractions were dried over Na<sub>2</sub>SO<sub>4</sub>. This was concentrated, and the resulting residue purified on silica column (2–20% EtOAc in hexane) to give 3.0 g (92%) of aldehyde **14** as an oil. <sup>1</sup>H NMR (400 MHz, CDCl<sub>3</sub>) δ 9.41 (s, 1H), 6.50 (td, *J* = 7.6, 1.0 Hz, 1H), 3.88–3.78 (m, 1H), 2.30 (t, *J* = 6.9 Hz, 2H), 1.89–1.79 (m, 2H), 1.75 (d, *J* = 0.4 Hz, 3H), 1.64–1.51 (m, 5H), 1.44–1.29 (dt, *J* = 14.5, 11.2 Hz, 2H). <sup>13</sup>C NMR (101 MHz, CDCl<sub>3</sub>) δ 195.16, 152.83, 140.31, 57.50, 36.46, 35.72, 29.22, 27.33, 9.41. IR (neat film) 2874, 2803, 2061, 1659, 1418, 1236 cm<sup>-1</sup>. HRMS (ESI) *m/z* calcd for C<sub>11</sub>H<sub>18</sub>N<sub>3</sub>O (M + H)<sup>+</sup>, 208.1445; found, 208.1455.

(3*R*,7*S*)-7-((1*E*,3*E*)-5-((1*S*,4*R*)-4-Azidocyclohexyl)-3-methylpent-1,3-dien-1-yl)-5,5-dimethyl-1,6-dioxaspiro[2.5]octane (**15**). A mixture of sulfone **5** (4.7 g, 13.4 mmol) and aldehyde **14** (2.4 g, 11.8 mmol) was concentrated with benzene (2 × 25 mL) under reduced pressure, dissolved in anhydrous THF (80 mL), and cooled to –78 °C. This stirred solution was treated dropwise with NaHMDS (14.7 mL, 1 M in THF, 14.7 mmol) over 10 min. The resulting yellow suspension was stirred at –78 °C for 1 h, allowed to warm in an ice bath for 15 min, and then allowed to warm to rt and stirred for 0.5 h. The reaction mixture was quenched with pH 7 buffer solution (120 mL) and extracted with Et<sub>2</sub>O (3 × 150 mL). The organic layer was dried (Na<sub>2</sub>SO<sub>4</sub>), filtered, and concentrated in vacuo. The solids were removed by filtration after the addition of 10% CH<sub>2</sub>Cl<sub>2</sub> in hexane. The resulting residue was purified on silica column (100 g, 2–20% EtOAc in hexane) to give 3.3 g (81%) of diene **15** (*E/Z* ratio 95:5) as an oil. <sup>1</sup>H NMR (400 MHz, CDCl<sub>3</sub>) δ 6.26 (d, *J* = 15.5 Hz, 1H), 5.54 (dd, *J* = 15.7, 6.7 Hz, 1H), 5.46 (t, *J* = 7.7 Hz, 1H), 4.51–4.39 (m, 1H), 3.82–3.72 (m, 1H), 2.57 (s, 2H), 2.10–2.02 (m, 2H), 2.02–1.86 (m, 2H), 1.84–1.73 (m, 3H), 1.71 (s, 3H), 1.59–1.46 (m, 4H), 1.42–1.38 (s,

3H), 1.30–1.24 (m, 2H), 1.27 (s, 3H), 1.25–1.12 (m, 2H). <sup>13</sup>C NMR (101 MHz, CDCl<sub>3</sub>) δ 136.19, 133.93, 131.74, 127.02, 73.01, 69.59, 57.94, 55.67, 51.03, 42.45, 38.62, 37.03, 34.88, 31.53, 29.24, 27.37, 27.32, 23.76, 12.50. IR (neat film) 2916, 2872, 2802, 2060, 1418, 1253, 956 cm<sup>-1</sup>. HRMS (ESI) *m/z* calcd for C<sub>20</sub>H<sub>32</sub>N<sub>3</sub>O<sub>2</sub> (M + H)<sup>+</sup>, 346.2489; found, 346.2492.

## ■ ASSOCIATED CONTENT

### Supporting Information

Full experimental details for the in vitro and in vivo biological methods, all details for the synthesis of all new compounds, and details for the single-crystal X-ray structure of compound **5**. This material is available free of charge via the Internet at <http://pubs.acs.org>.

## ■ AUTHOR INFORMATION

### Corresponding Author

\*E-mail: [thomasr.webb@gmail.com](mailto:thomasr.webb@gmail.com).

### Present Address

||SRI International, 333 Ravenswood Avenue, Menlo Park, California 94025-3493, United States. E-mail: [thomas.webb@sri.com](mailto:thomas.webb@sri.com). (Address as of January 2014.)

### Author Contributions

<sup>§</sup>These authors contributed equally to this work

### Notes

The authors declare no competing financial interest.

## ■ ACKNOWLEDGMENTS

We thank Peter Vogel, DVM, Ph.D. for the histopathologic evaluation of all tissues of animals subjected to infusions with sudemycin D6 during the MTD study and Christopher L. Morton for the generation of the xenograft model and the tumor-bearing animals used in this study. We also thank John Bollinger, Ph.D. for his determination of the high-resolution single-crystal X-ray structure of compound **5** and Christopher Calabrese, Ph.D. for his help in the establishment of the infusion model in mice. We thank Lei Yang of the High Throughput Analytical Chemistry Center for the compound plasma stability and compound solubility results. We also thank Alan Pourpak, Xiaoli Cui, and Dr. Steve Morris for the cytotoxicity data for the derivatives of compound **19**. This work was supported in part by NIH grant CA140474 and by the American Lebanese Syrian Associated Charities and St. Jude Children's Research Hospital.

## ■ ABBREVIATIONS USED

FR, FR901464; PD, pladienolide; HBTU, *N,N,N',N'*-tetramethyl-*O*-(1*H*-benzotriazol-1-yl)uronium hexafluorophosphate; NaHMDS, sodium bis(trimethylsilyl)amide; MeOH, methanol; EtOAc, ethyl acetate; AcOH, acetic acid; CI, combination index; CL, plasma clearance value; C<sub>max</sub>, maximum plasma concentration; EH, epoxide hydrolase; FBS, fetal bovine serum; JVC, jugular vein catheter; LLOQ, lower limit of quantification; MLEM, maximum likelihood via the expectation maximization algorithm; RSE, relative standard error; SEM, standard error of the mean; snRNPs, small nuclear ribonucleic particles; T<sub>max</sub>, time to reach C<sub>max</sub>; Tu<sub>vol</sub>, tumor volume

## ■ REFERENCES

(1) Kramer, A. The structure and function of proteins involved in mammalian pre-mRNA splicing. *Annu. Rev. Biochem.* **1996**, *65*, 367–409.

- (2) Golas, M. M.; Sander, B.; Will, C. L.; Luhrmann, R.; Stark, H. Molecular architecture of the multiprotein splicing factor SF3b. *Science* **2003**, *300*, 980–984.
- (3) Staley, J. P.; Guthrie, C. Mechanical devices of the spliceosome: Motors, clocks, springs, and things. *Cell* **1998**, *92*, 315–326.
- (4) Germann, S.; Grataudou, L.; Dutertre, M.; Auboeuf, D. Splicing programs and cancer. *J. Nucleic Acids* **2012**, *2012*, 269570-1–269570-9.
- (5) Nakajima, H.; Hori, Y.; Terano, H.; Okuhara, M.; Manda, T.; Matsumoto, S.; Shimomura, K. New antitumor substances, FR901463, FR901464 and FR901465. II. Activities against experimental tumors in mice and mechanism of action. *J. Antibiot.* **1996**, *49*, 1204–1211.
- (6) Nakajima, H.; Sato, B.; Fujita, T.; Takase, S.; Terano, H.; Okuhara, M. New antitumor substances, FR901463, FR901464 and FR901465. I. Taxonomy, fermentation, isolation, physico-chemical properties and biological activities. *J. Antibiot.* **1996**, *49*, 1196–1203.
- (7) Nakajima, H.; Takase, S.; Terano, H.; Tanaka, H. New antitumor substances, FR901463, FR901464 and FR901465. III. Structures of FR901463, FR901464 and FR901465. *J. Antibiot.* **1997**, *50*, 96–99.
- (8) Mizui, Y.; Sakai, T.; Iwata, M.; Uenaka, T.; Okamoto, K.; Shimizu, H.; Yamori, T.; Yoshimatsu, K.; Asada, M. Pladienolides, new substances from culture of *Streptomyces platensis* Mer-11107. III. In vitro and in vivo antitumor activities. *J. Antibiot.* **2004**, *57*, 188–196.
- (9) Asai, N.; Kotake, Y.; Nijijima, J.; Fukuda, Y.; Uehara, T.; Sakai, T. Stereochemistry of pladienolide B. *J. Antibiot.* **2007**, *60*, 364–369.
- (10) Kaida, D.; Motoyoshi, H.; Tashiro, E.; Nojima, T.; Hagiwara, M.; Ishigami, K.; Watanabe, H.; Kitahara, T.; Yoshida, T.; Nakajima, H.; Tani, T.; Horinouchi, S.; Yoshida, M. Spliceostatin A targets SF3b and inhibits both splicing and nuclear retention of pre-mRNA. *Nat. Chem. Biol.* **2007**, *3*, 576–583.
- (11) Kotake, Y.; Sagane, K.; Owa, T.; Mimori-Kiyosue, Y.; Shimizu, H.; Uesugi, M.; Ishihama, Y.; Iwata, M.; Mizui, Y. Splicing factor SF3b as a target of the antitumor natural product pladienolide. *Nat. Chem. Biol.* **2007**, *3*, 570–575.
- (12) Hasegawa, M.; Miura, T.; Kuzuya, K.; Inoue, A.; Won, K. S.; Horinouchi, S.; Yoshida, T.; Kunoh, T.; Koseki, K.; Mino, K.; Sasaki, R.; Yoshida, M.; Mizukami, T. Identification of SAP155 as the target of GEX1A (Herboxidiene), an antitumor natural product. *ACS Chem. Biol.* **2011**, *6*, 229–233.
- (13) Liu, X.; Biswas, S.; Berg, M. G.; Antapli, C. M.; Xie, F.; Wang, Q.; Tang, M. C.; Tang, G. L.; Zhang, L.; Dreyfuss, G.; Cheng, Y. Q. Genomics-guided discovery of thailandastatins A, B, and C as pre-mRNA splicing inhibitors and antiproliferative agents from *Burkholderia thailandensis* MSMB43. *J. Nat. Prod.* **2013**, *76*, 685–693.
- (14) Mandel, A. L.; Jones, B. D.; La Clair, J. J.; Burkart, M. D. A synthetic entry to pladienolide B and FD-895. *Bioorg. Med. Chem. Lett.* **2007**, *17*, 5159–5164.
- (15) Villa, R.; Mandel, A. L.; Jones, B. D.; La Clair, J. J.; Burkart, M. D. Structure of FD-895 revealed through total synthesis. *Org. Lett.* **2012**, *14*, 5396–5399.
- (16) Sakai, Y.; Tsujita, T.; Akiyama, T.; Yoshida, T.; Mizukami, T.; Akinaga, S.; Horinouchi, S.; Yoshida, M. GEX1 compounds, novel antitumor antibiotics related to herboxidiene, produced by *Streptomyces* sp. II. The effects on cell cycle progression and gene expression. *J. Antibiot.* **2002**, *55*, 863–872.
- (17) Webb, T. R.; Joyner, A. S.; Potter, P. M. The development and application of small molecule modulators of SF3b as therapeutic agents for cancer. *Drug Discovery Today* **2013**, *18*, 43–49.
- (18) Venables, J. P. Aberrant and alternative splicing in cancer. *Cancer Res.* **2004**, *64*, 7647–7654.
- (19) Kalnina, Z.; Zayakin, P.; Silina, K.; Line, A. Alterations of pre-mRNA splicing in cancer. *Genes, Chromosomes Cancer* **2005**, *42*, 342–357.
- (20) Bonnal, S.; Vigevani, L.; Valcarcel, J. The spliceosome as a target of novel antitumor drugs. *Nat. Rev. Drug Discovery* **2012**, *11*, 847–859.
- (21) Ogawa, S. Splicing factor mutations in myelodysplasia. *Int. J. Hematol.* **2012**, *96*, 438–442.
- (22) Damm, F.; Nguyen-Khac, F.; Fontenay, M.; Bernard, O. A. Spliceosome and other novel mutations in chronic lymphocytic leukemia and myeloid malignancies. *Leukemia* **2012**, *26*, 2027–2031.
- (23) Murati, A.; Brecqueville, M.; Devillier, R.; Mozziconacci, M. J.; Gelsi-Boyer, V.; Birnbaum, D. Myeloid malignancies: Mutations, models and management. *BMC Cancer* **2012**, *12*, 304.
- (24) Harbour, J. W.; Roberson, E. D.; Anbunathan, H.; Onken, M. D.; Worley, L. A.; Bowcock, A. M. Recurrent mutations at codon 625 of the splicing factor SF3B1 in uveal melanoma. *Nat. Genet.* **2013**, *45*, 133–135.
- (25) Hubert, C. G.; Bradley, R. K.; Ding, Y.; Toledo, C. M.; Herman, J.; Skutt-Kakaria, K.; Girard, E. J.; Davison, J.; Berndt, J.; Corrin, P.; Hardcastle, J.; Basom, R.; Delrow, J. J.; Webb, T.; Pollard, S. M.; Lee, J.; Olson, J. M.; Paddison, P. J. Genome-wide RNAi screens in human brain tumor isolates reveal a novel viability requirement for PHF5A. *Genes Dev.* **2013**, *27*, 1032–1045.
- (26) Gao, Y.; Koide, K. Chemical perturbation of Mcl-1 pre-mRNA splicing to induce apoptosis in cancer cells. *ACS Chem. Biol.* **2013**, *8*, 895–900.
- (27) Osman, S.; Albert, B. J.; Wang, Y.; Li, M.; Czaicki, N. L.; Koide, K. Structural requirements for the antiproliferative activity of pre-mRNA splicing inhibitor FR901464. *Chem.—Eur. J.* **2011**, *17*, 895–904.
- (28) Thompson, C. F.; Jamison, T. F.; Jacobsen, E. N. Convergent assembly of chiral components prepared by asymmetric catalysis. *J. Am. Chem. Soc.* **2000**, *122*, 10482–10483.
- (29) Horigome, M.; Motoyoshi, H.; Watanabe, H.; Kitahara, T. A synthesis of FR901464. *Tetrahedron Lett.* **2001**, *42*, 8207–8210.
- (30) Thompson, C. F.; Jamison, T. F.; Jacobsen, E. N. FR901464: Total synthesis, proof of structure, and evaluation of synthetic analogues. *J. Am. Chem. Soc.* **2001**, *123*, 9974–9983.
- (31) Albert, B. J.; Sivaramakrishnan, A.; Naka, T.; Koide, K. Total synthesis of FR901464, an antitumor agent that regulates the transcription of oncogenes and tumor suppressor genes. *J. Am. Chem. Soc.* **2006**, *128*, 2792–2793.
- (32) Albert, B. J.; Sivaramakrishnan, A.; Naka, T.; Czaicki, N. L.; Koide, K. Total syntheses, fragmentation studies, and antitumor/antiproliferative activities of FR901464 and its low picomolar analogue. *J. Am. Chem. Soc.* **2007**, *129*, 2648–2659.
- (33) Lagisetti, C.; Pourpak, A.; Jiang, Q.; Cui, X.; Goronga, T.; Morris, S. W.; Webb, T. R. Antitumor compounds based on a natural product consensus pharmacophore. *J. Med. Chem.* **2008**, *51*, 6220–6224.
- (34) Lagisetti, C.; Pourpak, A.; Goronga, T.; Jiang, Q.; Cui, X.; Hyle, J.; Lahti, J. M.; Morris, S. W.; Webb, T. R. Synthetic mRNA splicing modulator compounds with in vivo antitumor activity. *J. Med. Chem.* **2009**, *52*, 6979–6990.
- (35) Fan, L.; Lagisetti, C.; Edwards, C. C.; Webb, T. R.; Potter, P. M. Sudemycins, novel small molecule analogues of FR901464, induce alternative gene splicing. *ACS Chem. Biol.* **2011**, *6*, 582–589.
- (36) Gundluru, M. K.; Pourpak, A.; Cui, X.; Morris, S. W.; Webb, T. R. Design, synthesis and initial biological evaluation of a novel pladienolide analog scaffold. *MedChemCommun* **2011**, *2*, 904–908.
- (37) Jennings, L.; Murphy, G. M. Predicting outcome in melanoma: where are we now? *Br. J. Dermatol.* **2009**, *161*, 496–503.
- (38) Smith, A. B., 3rd.; Dong, S.; Brenneman, J. B.; Fox, R. J. Total synthesis of (+)-sorangicin A. *J. Am. Chem. Soc.* **2009**, *131*, 12109–12111.
- (39) Lawrence, N. J.; Drew, M. D.; Bushell, S. M. Polymethylhydroxiloxane: A versatile reducing agent for organic synthesis. *J. Chem. Soc., Perkin Trans. 1* **1999**, *0*, 3381–3391.
- (40) Goddard-Borger, E. D.; Stick, R. V. An efficient, inexpensive, and shelf-stable diazotransfer reagent: Imidazole-1-sulfonyl azide hydrochloride. *Org. Lett.* **2007**, *9*, 3797–3800.
- (41) Ye, H.; Liu, R.; Li, D.; Liu, Y.; Yuan, H.; Guo, W.; Zhou, L.; Cao, X.; Tian, H.; Shen, J.; Wang, P. G. A safe and facile route to imidazole-1-sulfonyl azide as a diazotransfer reagent. *Org. Lett.* **2012**, *15*, 18–21.

(42) Lehar, J.; Krueger, A. S.; Avery, W.; Heilbut, A. M.; Johansen, L. M.; Price, E. R.; Rickles, R. J.; Short, G. F., 3rd.; Staunton, J. E.; Jin, X.; Lee, M. S.; Zimmermann, G. R.; Borisy, A. A. Synergistic drug combinations tend to improve therapeutically relevant selectivity. *Nat. Biotechnol.* **2009**, *27*, 659–666.

(43) Maira, S. M.; Stauffer, F.; Brueggen, J.; Furet, P.; Schnell, C.; Fritsch, C.; Brachmann, S.; Chene, P.; De Pover, A.; Schoemaker, K.; Fabbro, D.; Gabriel, D.; Simonen, M.; Murphy, L.; Finan, P.; Sellers, W.; Garcia-Echeverria, C. Identification and characterization of NVP-BEZ235, a new orally available dual phosphatidylinositol 3-kinase/mammalian target of rapamycin inhibitor with potent in vivo antitumor activity. *Mol. Cancer Ther.* **2008**, *7*, 1851–1863.

(44) LoPiccolo, J.; Blumenthal, G. M.; Bernstein, W. B.; Dennis, P. A. Targeting the PI3K/Akt/mTOR pathway: Effective combinations and clinical considerations. *Drug Resist. Updates* **2008**, *11*, 32–50.

(45) Liu, J. Y.; Park, S. H.; Morisseau, C.; Hwang, S. H.; Hammock, B. D.; Weiss, R. H. Sorafenib has soluble epoxide hydrolase inhibitory activity, which contributes to its effect profile in vivo. *Mol. Cancer Ther.* **2009**, *8*, 2193–2203.

(46) Decker, M.; Arand, M.; Cronin, A. Mammalian epoxide hydrolases in xenobiotic metabolism and signalling. *Arch. Toxicol.* **2009**, *83*, 297–318.

(47) Chou, T. C.; Talalay, P. Quantitative analysis of dose-effect relationships: The combined effects of multiple drugs or enzyme inhibitors. *Adv. Enzyme Regul.* **1984**, *22*, 27–55.

(48) Laizure, S. C.; Herring, V.; Hu, Z.; Witbrodt, K.; Parker, R. B. The role of human carboxylesterases in drug metabolism: Have we overlooked their importance? *Pharmacotherapy* **2013**, *33*, 210–222.

(49) Fischer, N.; Goddard-Borger, E. D.; Greiner, R.; Klapötke, T. M.; Skelton, B. W.; Stierstorfer, J. Sensitivities of some imidazole-1-sulfonyl azide salts. *J. Org. Chem.* **2012**, *77*, 1760–1764.